arXiv:1607.01304v1 [astro-ph.SR] 5 Jul 2016

Cool Subdwarf Investigations III: Dynamical Masses of Low Metallicity Subdwarfs

Wei-Chun Jao[1]

Department of Physics and Astronomy, Georgia State University, Atlanta, GA 30302

jao@astro.gsu.edu

Ed. P. Nelan

Space Telescope Science Institute, 3700 San Martin Drive, Baltimore, MD 21218, USA

nelan@stsci.edu

Todd J. Henry[1]

RECONS Institute, Chambersburg, PA 17201

thenry@astro.gsu.edu

Otto G. Franz, Lawrence H. Wasserman

Lowell Observatory, 1400 West Mars Hill Road, Flagstaff, AZ 86001

ogf@lowell.edu, lhw@lowell.edu

Received _____; accepted _____

submitted to *Astronomical Journal (v.0628.2016)*

[1]Visiting Astronomer, Cerro Tololo Inter-American Observatory. CTIO is operated by AURA, Inc. under contract to the National Science Foundation.

ABSTRACT

We report dynamical mass measurements for the components of the previously known double-lined spectroscopic subdwarfs G 006-026 B and C using the Fine Guidance Sensors (FGS) on the *Hubble Space Telescope*. To build the empirical mass-luminosity relation for low metallicity subdwarfs, we collect four other subdwarf systems with dynamical masses that we compare to theoretical models for various metallicities on the mass-luminosity relation. For most stars, they fall in the regions where the models predict to be low metallicity. This effort highlights the scarcity of dynamical masses for subdwarfs and that much work remains to be done to improve the mass errors and metallicity measurements of low mass subdwarfs in our Galaxy.

Subject headings: astrometry — solar neighborhood — stars: distances — stars: late-type — (stars:) subdwarfs

1. Introduction

Subdwarfs are Galactic fossils that presumably comprise the bulk of the halo, and are crucial touchstones of the star formation and metal enrichment histories of the Milky Way. The local paucity of subdwarfs and their intrinsic faintness make them difficult to characterize, unlike their disk counterparts. For example, there are currently only three confirmed subdwarf systems within 10 parsecs: μ Cas AB, CF UMa, and Kapteyn's Star (Monteiro et al. 2006). Many subdwarfs are detected via high proper motion star surveys (e.g. Ryan & Norris 1991, Carney et al. 1994, Gizis 1997, Jao et al. 2005, 2008, Lépine et al. 2007, and Savcheva et al. 2014), yielding important information about their kinematics, chemical compositions, and space densities. However, their masses — the single most important parameter for a star — are still mostly unknown, but would be of great use in studies of the Galactic halo, globular clusters, and other old and/or low metallicity systems.

There are currently only a half dozen subdwarf systems (here defined as stars having [m/H] or [Fe/H]≤ -0.5) with dynamical mass measurements. McCarthy et al. (1993) used infrared speckle interferometry and Drummond et al. (1995) used Adaptive Optics to measure the masses of μ Cas AB, which has [Fe/H]$= -0.71$ (Karaali et al. 2003) and is one of the nearest subdwarf systems. Söderhjelm (1999) reported masses for GJ 704 AB (99 Her), which has [Fe/H]$= -0.58$ (See Table 5). Recently, Horch et al. (2015) reported total masses for two subdwarf binaries (HIP 85209AB and HIP 95575AB) using the Differential Speckle Survey Instrument (DSSI) to resolve these two doubled-lined spectroscopic binaries (Goldberg et al. 2002; Halbwachs et al. 2012). We use the mass-ratio from SB2 results and total masses from Horch et al. (2015) to get individual masses. All of these results are summarized in Table 1. We note that HIP 81023AB and HIP 103987AB both have metallicity less than -0.5, but have preliminary orbital results from Horch et al. (2015).

We did not include them in our analysis. Ren & Fu (2013) combined both single-lined spectroscopic data, photocentric orbital data from the Hipparcos Intermediate Astrometric Data and an empirical mass-luminosity relation to estimate masses for four additional subdwarf systems with [Fe/H]≤ -0.5 (HIP 705, HIP 39893, HIP 55022, HIP 59750 and HIP 73440). However, these masses are not measured dynamically, as they rely on an empirical mass-luminosity relation from stars with solar metallicity, so these stars are not included in our discussion. Finally, Söderhjelm (1999) reported the total system mass and mass ratio of GJ 60AB with [Fe/H]$= -0.65$ (Holmberg et al. 2009). A few years later, Watson et al. (2001) reported that the system could harbor four components rather than two, with close binaries A-C and B-D, where B-D is an eclipsing binary with a period of 0.45 days. Because of the complexity of this system, we conclude that no reliable masses for individual components have been measured, so do not include this system in the discussion.

Nearby galactic globular clusers (GCs) are also homes of low metallicities stars. Recently, the Clusters AgeS Experiment (CASE) project (Kaluzny et al. 2015, and references therein) has detected and measured many detached eclipsing binaries in ω Cen, 47 Tuc, M4, M55 and NGC6362. These binaries are comprised of either massive or evolved stars, and their metallicities are much lower than nearby field subdwarfs, so they are not discussed further in this paper either.

Because the local known subdwarf density is far less than that for dwarfs, coupled with the fact that the multiplicity of cool subdwarfs appears to be lower than that of main sequence stars (Jao et al. 2009; Lodieu et al. 2009), it has been difficult to identify appropriate binary systems to target for dynamical mass determinations. This is particularly true for low mass M-type subdwarfs with masses less than 0.6 $M_{\odot}$. Consequently, the number of dynamical masses measured for low metallicity subdwarfs is much less than for their counterparts, the main sequence dwarfs (Henry et al. 1999; Delfosse et al. 2000;

Torres et al. 2010; Benedict et al. 2016). Building an empirical mass-luminosity relation for low metallicity stars has proven difficult, and rigorous testing of low metallicity theoretical models remains to be done. In this manuscript, we present new dynamical masses of ∼0.47 and 0.44 $M_{\odot}$ for the low metallicity subdwarfs, G 006-026 B and C, adding two subdwarf masses to establish the empirical mass-luminosity relation. We also recalculate the masses for GJ 704 A and B by reassessing the resolved measurements to date.

G 006-026 BC ia a double-lined spectroscopic binary with period of about 302 days (Goldberg et al. 2002). Carney et al. (1994) reported that the primary star in the system, the G-type star G 006-026 A, has a metallicity of $[m/H] = -0.88$. Later, Casagrande et al. (2011) and Holmberg et al. (2009) use photometry to determine the primary's $[Fe/H] = -0.52$ and -0.60, respectively. We assume that the B and C components have the same metallicity as the primary, and that they therefore meet our criterion for subdwarfs as stars having [Fe/H]≤ -0.5. Five of the seven orbital elements have been determined: period (P), time of the periastron (T), semi-major axis (a), eccentricity (e) and position of periastron (ω). The binary's orbital inclination (i) and longitude of the ascending of node (Ω) remain unknown from spectroscopic data alone. Because of its relatively large $a \sin i$ value among the 34 SB2 systems in Goldberg et al. (2002), we expected the Fine Guidance Sensor on the Hubble Space Telescope to be able to resolve the system at appropriate orbital phases. By accurately measuring the angular separation of the two components at only a few epochs, we can reliably determine all of the orbital elements and thus the individual masses of the B and C components.

Table 1. Metallicities and Dynamical Masses of Subdwarfs

Name	π mas	[m/H]	[Fe/H]	Ref.	Mass (A) $M_\odot$	M_V	Mass (B) $M_\odot$	M_V	Ref.
HIP 85209 AB	19.76±0.82	$(-0.75)^b$		2	0.84±0.09	5.42	0.74±0.10	5.41	1[a]
HIP 95575 AB	39.98±0.73	−0.80		3	0.69±0.10	6.80	0.58±0.09	7.03	1[a]
μ Cas AB	132.67±0.74		−0.71	9	0.742±0.059	5.78	0.173±0.011	11.6	4
GJ 704 AB	64.30±0.68		−0.58	6	0.89 ± 0.03^c	4.16	0.51 ± 0.03^c	7.46	5
G 006-026 BC	25.67±0.04	−0.88		8	0.474±0.053	10.34	0.436±0.049	10.64	7

Note. — All parallaxes other than μ Cas AB and GJ704 AB are from van Leeuwen (2007). The weighted mean parallax of μ Cas AB is from van Leeuwen (2007) and van Altena et al. (1995). The weighted mean parallax of GJ704AB is from van Altena et al. (1995) and Söderhjelm (1999). [a]Horch et al. (2015) did not report individual mass errors, but they have total mass ($M_A + M_B$) errors. We adopt these total mass errors to get errors in percentage of masses and apply them to each component. [b]The metallicity of HIP 85209 is discussed in §6. [c]The

masses of GJ 704 AB are discussed in §4 and details are given in Table 4

References. — (1) Horch et al. (2015), (2) Latham et al. (1992), (3) Holmberg et al. (2009), (4) Drummond et al. (1995), (5) Söderhjelm (1999), (6) mean value of several measurements given in Table 5, (7) this work, (8) Carney et al. (1994), (9) Karaali et al. (2003)

2. Observations and Results

We utilized one of *Hubble Space Telescope's* three Fine Guidance Sensors (HST/FGS1r, hereafter simply FGS) in its TRANS mode to resolve G 006-026 BC. The FGS is a white light shearing interferometer. When operated in it high angular resolution TRANS mode, it scans a luminous source and produces interference fringes along two orthogonal axis (X and Y). Resolved binary systems yield interference fringes, or S-curves, that have reduced amplitude and different morphology than those of point sources (unresolved stars). Model binary systems, built from point source templates, are used to determine the projected separation and relative bightness of the binary components along both the FGS X and Y axis. We carried out TRANS mode observations of G 006-026 BC during *HST* Cycles 15 and 19 to measure the separations and position angles for the C component relative to B at six epochs. Typically, we scheduled 30–32 scans on both X and Y axes during each visit, with scan lengths of $0\farcs4$–$1\farcs0$ on either side of the target. Observations were made through the F583W filter, which provides magnitude differences similar to the V_J band in the Johnson system (hereafter, simply V).

The spectroscopic data (Goldberg et al. 2002), available mass estimates, and the Hipparcos distance to G 006-026 A indicated that the maximum separation of the two stars would be ±25 milli-arcseconds (mas). However, because we did not know the position angle of the binary (due to lack of knowledge of orbit's inclination and longitude of ascending node), it was not possible to select with certainty an orientation of the *HST* that would guarrentee that the binary would be resolved along both axes of the FGS, which has a per axis angular resolution close to 10 mas. For the first observation in 2006, we selected an observation date that corresponded to a time of maximum separation assuming an inclination of 45 degrees, but still with no knowledge of the longitude of ascending node. The binary was well resolved along the FGS X-axis but unresolved along the Y-axis. The

observed separation along the X axis allowed for an estimate of the system's inclination but left a position angle uncertainty of about +/- 27 degrees (because the actual Y-axis separation can be anywhere from +/-10 mas). Subsequent observations in 2011 through 2014 were planned using the spectroscopic orbital elements combined with the FGS data previously acquired. For our last epoch in 2014, we observed the binary in two consecutive *HST* orbits with a telescope roll change of 41 degrees between them in an attempted to resolve the system along both FGS axes, or to at least tightly constrain the binary position angle.

The standard *strfits* routine in the IRAF/STSDAS package was used to convert the archived TRANS mode FITS files into GEIS files (generic edited information sets, the original file structure used for the legacy *HST* instrument calibration pipelines, but still in use for FGS). For each visit these GEIS data were processed through the FGS raw data processing routine *calfgsa*, resulting in sets of individual interference scans in the X and Y directions across the binary. The analysis package *ptrans* was then used to cross-correlate, and co-add the individual scans, and to smooth the final co-added X and Y axis scans for each visit. Additional details of the reduction procedure can be found in the *HST/FGS Data Handbook* (http://www.stsci.edu/hst/fgs/documents/datahandbook/).

The analysis of FGS TRANS mode observations of binary stars requires the availabilty of TRANS mode observations of single (point source) calibration stars of similar color. In January 2009 the FGS1r internal optics were re-aligned to re-optimize (change) the instrument's interferometric response. Thus our early 2006 epoch observation uses SAO 185689 as the calibration star, which was observed in 2006, while all later epochs use LHS 73, which was observed in 2009 after the FGS re-optimization. The same data processing routines and packages discussed above were applied to these calibaration stars. Routine monitoring of FGS TRANS mode performance by STScI indicates that its interference

fringes have not changed since FGS's realignment in 2009, so use of LHS 73 data from 2009 as the point source template for the later epochs is justified. We note that LHS 73 ($V - K_s$ =3.44) is a known low metallicity K6 subdwarf (Jao et al. 2008) with a similar color to G 006-026 BC ($V - K_s$ =4.14). Two other often used FGS calibrators, Latcol-A and HD233877, do not yield better fits/residuals than LHS 73, so we use LHS 73 as our calibrator.

Finally, we used the standard *binary_fit* package discussed in the *HST FGS Data Handbook* to compare the interference fringes, or S-curves, of G 006-026 BC to the calibrators to calculate the best fitting component magnitude difference and separations in the X and Y directions. Figure 1 shows an example fitting result for both axes in 2013.09. The *binary_fit* program yields the best Δm and separation by comparing with the calibrator. However, we notice that the fitting for this system is not sensitive to the Δm for all scans as shown in Figure 2. Because of this reason, we fix the Δm at 0.3 with an error of 0.3 mag and apply this fixed value for all other scans while we use *binary_fit* routine.

We converted these separations along the FGS axes to separations ρ and position angles θ on the sky using the *HST* keyword PA_APER in the GEIS header, which is the position angle of the FGS Y-axis at the time of the observation. Results for the six epochs of observation are given in Table 2. Measurement errors in the ρ and θ are shown in parenthess. For epochs 2006.55227 and 2011.83228 the binary was only resolved along one of FGS axis, therefore the resultant uncertainty in position angle is large (assuming up to 10 mas uncertainty in separation along the unresolved axis). The data acquired in 2014 has the binary marginally resolved along the FGS Y-axis. For such small separations, solutions of the opposite parity must be considered (i.e., a separation of -12.4 mas is nearly indistinguishable from a separation of +12.4 mas). However, a different parity of the Y-axis separation for either of the two visits produces incompatible position angles (205.26 degrees

for the first visit, 299.63 degress for the second visit). Thus by having changed the *HST* roll angle by 41 degrees between the two visits, we are able to select the correct parity and tightly constrain the binary position angle at this epoch.

3. G 006-026 BC

We used the MIIPS (Multipurpose Interactive Image Processing System, (Gudehus 2001)) package to calculate all seven orbital elements and as well as dynamical masses for the B and C components by using the FGS results from this work and radial velocities from Goldberg et al. (2002). The radial velocity dataset includes 43 epochs/observations taken with the Center for Astrophysics Digital Speedometers, which provide velocities with residuals on the order of 1 km/s. The radival velocity data are shown in Figure 3, with the fit to the data from our work. A total of five epochs of astrometric data from the FGS is used to complete the determination of the systems orbital elements. Figure 4 shows the plot of G 006-026 BC's relative orbit. Table 3 shows our fit to the orbital elements along with those from Goldberg et al. (2002).

There are four (P, e, ω, T) orbital elements and γ (system velocity) from this work in common with measurements from Goldberg et al. (2002), and all are generally consistent. However, because this system is a challenge to resolve with FGS, the error in orbital inclination (4.98°) is relatively large and results in larger mass errors (11%) than anticipated. By combining the visual and spectroscopic orbits, we measure a high-quality orbital parallax of $0\farcs02634\pm0\farcs0002$, placing the system at 37.9 pc. This is consistent with the trigonometric parallax measured by *Hipparcos* for the primary, G 006-026 A, $0\farcs02561\pm0\farcs00134$ (van Leeuwen 2007).

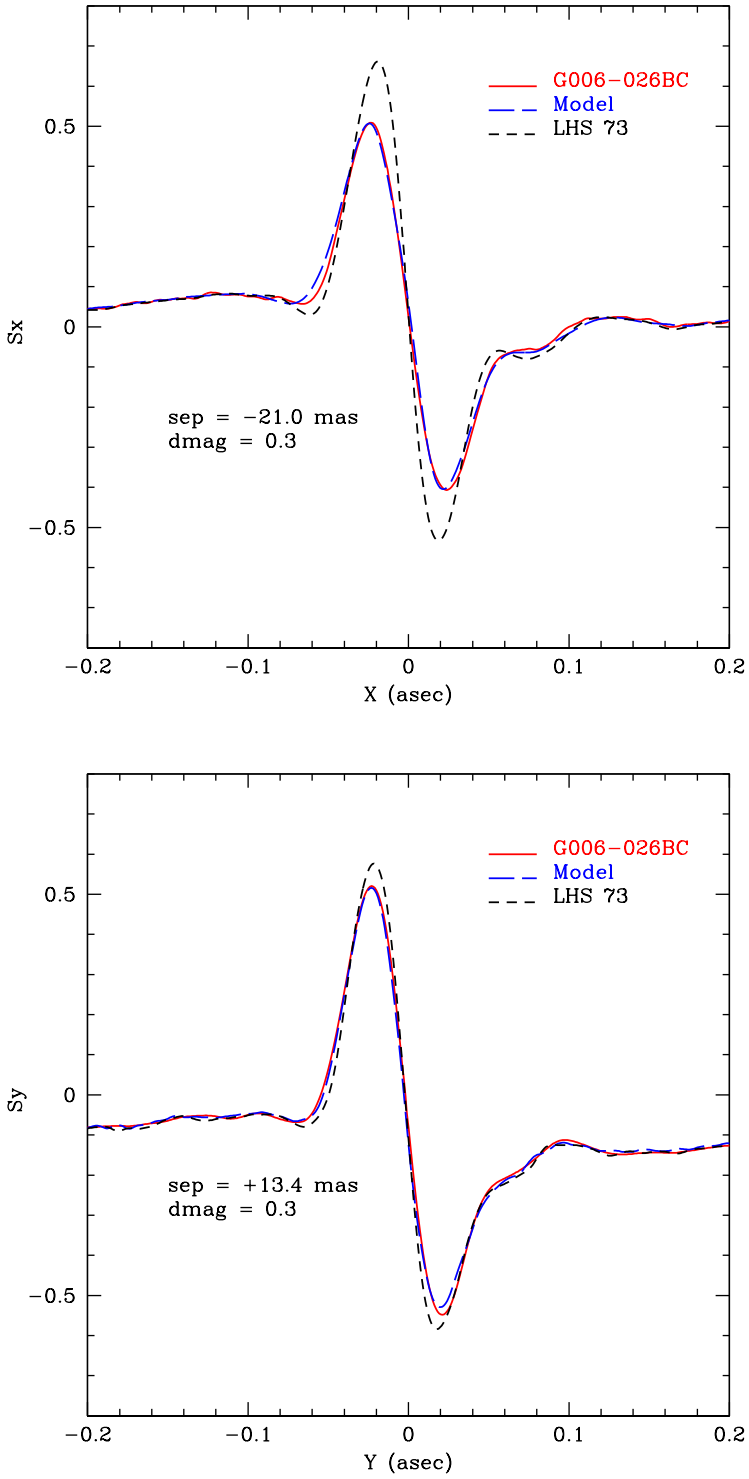

Fig. 1.— The FGS X and Y axis interference fringes for the observation of G 006-026 BC and the best fitting model are shown. For perspective, the interference fringes for the point source calibration star LHS 73 are also shown. The Y-axis separation of 13.4 mas approaches the 10 mas angular resolution limit of the FGS.

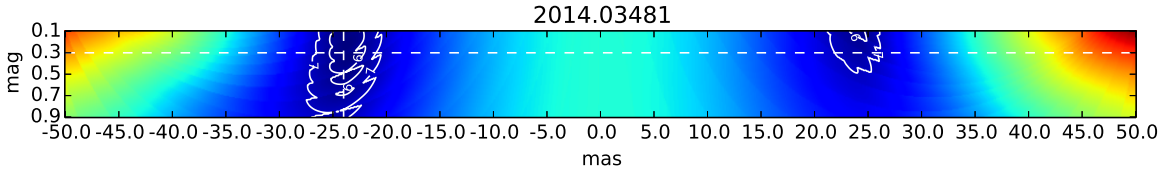

Fig. 2.— This color plot shows the residuals of the fitting while changing the Δm and separation of the secondary in 2014.03481. Residuals rise from blue to red. Two white contours represent the equal residuals of the two lowest residuals 6 (inner contour) and 7 (outer contour). Two dashed lines indicate the location of the best fit from *binary_fit* routine.

Table 2. HST/FGS TRANS mode results

epoch	X sep	Y sep	PA Aper	ρ	θ
	mas	mas	deg	mas	deg
2006.55227	+22.7	-7.0	170.6	23.8(2)	277.7(27)
2011.83228	+8.9	18.5	170.2	20.6(2)	195.9(33)
2013.09010	-21.0	13.4	344.0	24.9(2)	286.6(5)
2013.12103	-20.8	13.1	337.0	24.6(2)	279.3(5)
2014.03481 *	-21.7	12.4	325.0	24.8	265.0
2014.03498 *	-24.0	-10.5	6.0	26.2	252.0

*We combine these two epochs of data to get a mean separation (25.5±2 mas) and position (258.5±7°) angle in 2014.0349 for our orbital fitting routine. The individual errors of ρ and θ of these two epochs are not shown in this table.

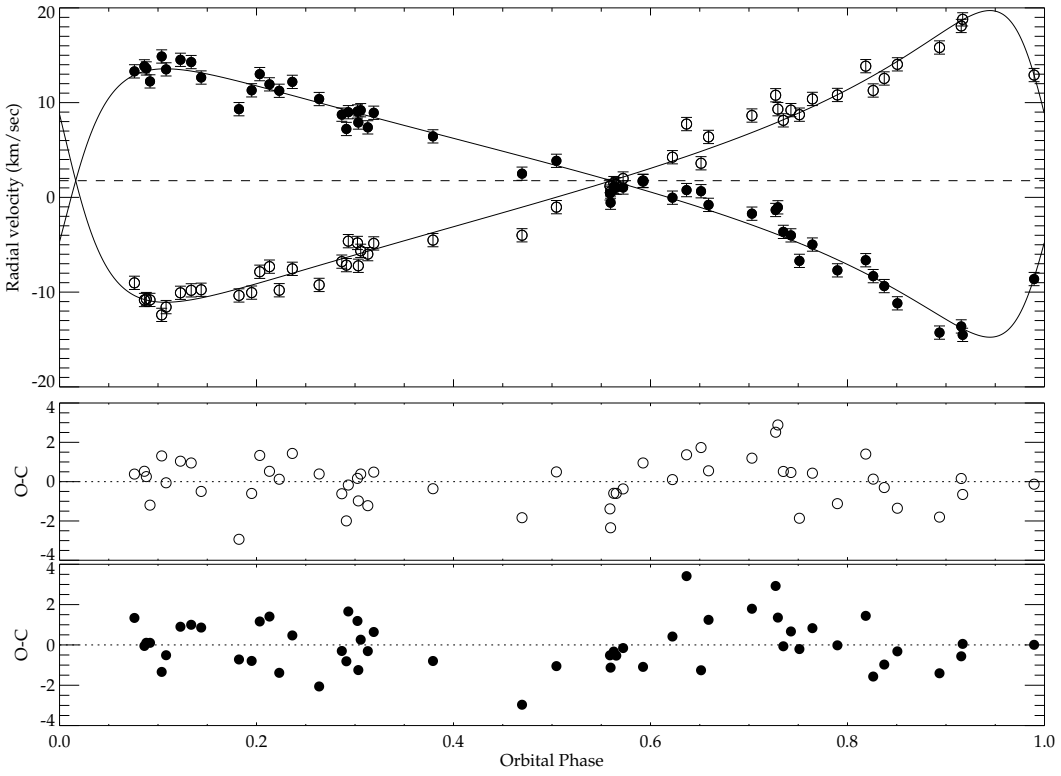

Fig. 3.— The radial velocity data for G 006-026 BC from Goldberg et al. (2002). Filled and open circles are for the primary and secondary velocities, respectively. Residuals are shown on the bottom of the figure for both primary and secondary. Because there is no error available for individual radial velocity measurements, the mean error of 0.7 km/sec is uses for all measurments.

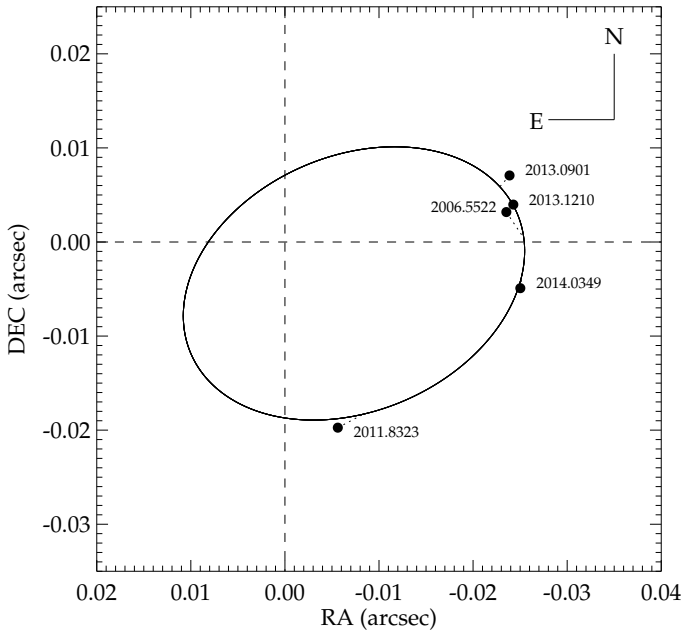

Fig. 4.— The relative orbital motion of G 006-026 BC is shown using the FGS results. Dashed lines connect observed and calculated positions.

Table 3. Orbital elements of G 006-026 BC

Parameters	Goldberg	this work
Period (P yr)	0.826±0.001	0.826±0.0003
Semi-major axis (a $''$)	···	0.0108±0.0004
Eccentricity (e)	0.582±0.017	0.577±0.004
Inclination (i °)	···	128.31±4.98
Ascending Node (Ω °)	···	123.12±3.42
Longitude of Periastron (ω °)	252.8±1.9	253.24±0.46
Epoch of Periastron (T yr)	1991.4385±0.004	1991.4394±0.0008
System Velocity (γ km sec^{-1})	1.76±0.12	1.76±0.03
Primary Amplitude ($K1$ km sec^{-1})	14.25±0.42	14.16±1.44
Primary Amplitude ($K2$ km sec^{-1})	15.48±0.44	15.39±1.57
Parallax (π $''$)	···	0.02634±0.0002
Total Mass ($M_\odot$)	···	0.911±0.110
$M_{A\odot}$	···	0.474±0.053
$M_{B\odot}$	···	0.436±0.049

4. GJ 704 AB

GJ 704 AB is a visual binary with a ∼56 year orbital period at 15.6 pc. The first visual measurement of the system dates back to 1859 (Mason et al. 2015). Heintz (1972), Söderhjelm (1999), and Kennedy et al. (2012) have all calculated orbits and individual masses for the components, while Malkov et al. (2012) reported a total mass for the system. The system is also a single-lined spectroscopic binary (SB1), with an orbit published by Abt & Willmarth (2006). Orbital results for all five studies are given in Table 4.

As of 2015, the Washington Double Star (WDS) catalog (Mason et al. 2015) lists 240 different epochs of observations for GJ 704 AB, with the most recent measurement being that of Kennedy et al. (2012). After removing epochs with uncertain measurements and large errors, we have adopted a dataset including 204 total measurements spanning 1859–2011 (i.e the same coverage as Kennedy et al. (2012)), and recalculate the relative orbit by combining both WDS resolved measurements and the radial velocity data from Abt & Willmarth (2006). For a given WDS epoch, we assign a weight for the astrometric position based on telescope aperture, system separation, and/or magnitude difference, following the prescription of Hartkopf et al. (2001). Table 4 lists our new set of orbital elements, which are consistent with previous efforts. Our resulting orbital fit is shown in Figure 5, where it is clear that there are few reliable measurements near periastron. We use the period and semi-major axis of this orbit and the weighted mean parallax of 64.3 mas from van Altena et al. (1995) and Söderhjelm (1999) to derive a total mass for the system of 1.40 ± 0.03 $M_\odot$.

With the total system mass and orbital elements in hand, there are two ways to calculate the masses of the components. First, we use the mass function ($f(m)$ =0.01273) of the SB1 reported by (Abt & Willmarth 2006) to determine individual masses of 0.91 $M_\odot$ and 0.48 $M_\odot$. Second, we use $\Delta V = 3.3$ mag and the photocentric semi-major axis of 0.″353

from Heintz (1972) to calculate the scale of the photocentric/relative orbit that yields the mass fraction, f *or* $M_B/(M_A + M_B) = 0.379$. Given the total mass, we then find masses of 0.86 $M_\odot$ and 0.53 $M_\odot$ for the components. For the final masses, we adopt the means of these two methods, and find masses of 0.89 $M_\odot$ and 0.51 $M_\odot$. The mean difference between these mean values, 0.03$M_\odot$, is adoped as their errors, as listed in Table 4.

According to SIMBAD, fifty-five publications report abundances for GJ 704 AB since 1960. Determining which [Fe/H] values are best is a monumental task beyond the scope of this manuscript. We select four measurements of [Fe/H] reported in refereed publications during the past 10 years and [Fe/H] measurements, including both spectroscopic and photometric methods. These measurements are given in Table 5, where we list a mean value of [Fe/H] = -0.58[1] that indicates this to be a low-metallicity binary. We note only Holmberg et al. (2009) used photometry to measure [Fe/H].

5. M_V Values as Proxies for Luminosities

To develop an empirical mass-luminosity relation for subdwarfs we use M_V in the Johnson system as a proxy for luminosity. Two systems, μ Cas AB and GJ 704 AB, have combined V, ΔV, and parallax measurements, so it is straightforward to obtain individual V magnitudes for each component. However, the two subdwarf systems from Horch et al. (2015) have Δm_{692nm} and Δm_{880nm} rather than ΔV measurements. To convert Δm_{692} from this special narrow band to the V filter, we may (1) use synthetic spectra for low metallicity stars convolved with filter passbands to convert from Δm_{692nm} to ΔV, or (2) build an empirical relation from existing systems with both Δm_{692} and ΔV measurements. The first

[1]Latham and Bieryla (2016) similarly reports that the [Fe/H] of GJ 704 AB is -0.59 according to their unpublished data.

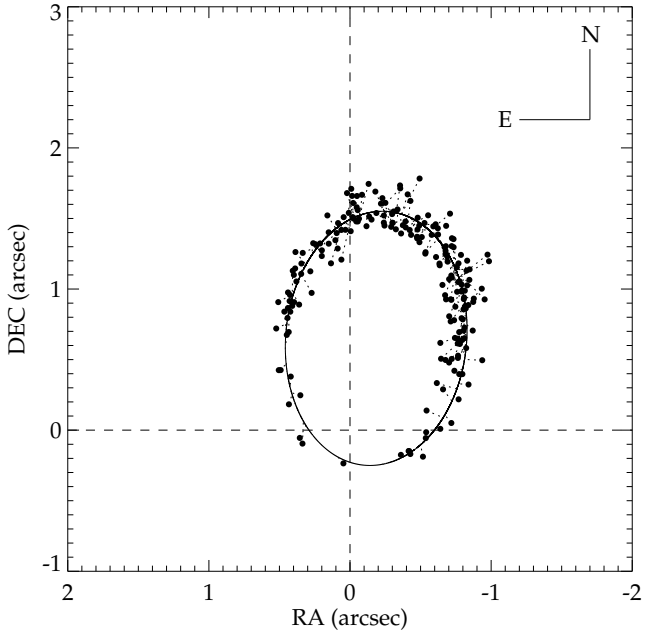

Fig. 5.— The relative orbital motion of GJ 704 AB is shown using data from the WDS. Dashed lines connect observed and calculated positions.

Table 4. Orbital Elements for GJ 704 AB

Parameters	Heintz (1972)	Söderhjelm (1999)	Malkov (2012)	Kennedy (2012)	Abt (2006)	this work
Period (P yr)	55.8	56.4	56.04	56.3	56.4(fixed)	55.91±0.12
Semi-major axis (a ″)	1.00	1.00	1.123	1.06	···	1.05±0.02
Eccentricity (e)	0.74	0.75	0.798	0.766	0.75(fixed)	0.761±0.007
Inclination (i °)	32.0	34.0	···	39	···	36.18±1.72
Ascending Node (Ω °)	218.7	216.0	···	41	···	223.62±3.21
Longitude of Periastron (ω °)	300.6	301.0	···	116	120.4	295.38±2.84
Epoch of Periastron (T yr)	1941.8	1998.0	···	1997.62	1999.52	1997.8±0.09
Parallax (π ″)	0.064	0.0639	0.06393	0.06393	···	0.0643±0.00068
Total Mass ($M_\odot$)	1.49	1.25	1.73	1.4	···	1.40±0.03
Astrometric Coverage (yr)	1859–1968	1859?–1997?	unknown	1859–2011	1988–1996 (V_{rad})	1859–2011
$M_{A\odot}$	0.90	(0.75)	···	0.94	···	0.89
$M_{B\odot}$	0.59	(0.50)	···	0.46	···	0.51

Note. — The span of astrometric coverage is for visual relative positions, rho and θ, except in the case of Abt & Willmarth (2006), where the duration of the radial velocity measurements is given. The astrometric coverage for Söderhjelm (1999) is estimated to be up to 1997, which is the latest astrometric reference in that paper. We use $f = 0.4$ and the total mass from Söderhjelm (1999) to estimate individual masses for that effort. Malkov et al. (2012) do not clearly state the timespan of observations used for their analysis. We note that the total masses are different between Heintz (1972) and Söderhjelm (1999), even though their orbital elements are essentially identical. The values in this table are directly from their papers. Based on Kepler 3^{rd} law, the total masses should be 1.49 and 1.25, respectively for Heintz (1972) and Söderhjelm (1999).

Table 5. Metallicity Values for GJ 704 AB

Publications	[Fe/H]
Takeda & Takada-Hidai (2013)	−0.58
Maldonado et al. (2012)	−0.6
Korotin et al. (2011)	−0.6
Holmberg et al. (2009)	−0.55
mean	−0.58

method requires knowing the metallicity of each system and the spectral types or effective temperatures of each component so that we can select corresponding synthetic spectra with the same $[m/H]$ and T_{eff}. However, in order to make a direct comparison between empirical and model mass-luminosity relations, here we try to limit the use of synthetic spectra to derive any stellar parameters, including V, so we use the second method.

To create a reliable conversion from Δm_{692} to ΔV, we first searched the WDS for systems with both measurements. Unfortunately, we found no such systems, but we did find 51 systems with both Δm_{692} and ΔV_{Tycho} measurements. A linear relation between measurements through these two filters is shown in Figure 6.

Ideally, we would then convert ΔV_{Tycho} to ΔV using the polynomial conversion provided by (Mamajek et al. 2002). However, this conversion requires the $B_T - V_T$ colors of each star, which is currently unavailable for any of two systems. Nonetheless, we note that the error in our relation shown in Figure 4 is ∼0.46 mag between ΔV_{Tycho} and Δm_{692}, which is much larger than the conversion error between Johnson V and V_{Tycho}. Therefore, until direct ΔV measurements are available, we assume $\Delta V_{Tycho} \approx \Delta V$ for the two subdwarf systems in Horch et al. (2015) and adopt ∼0.46 mag for our V errors.

The G 006-026 BC system targeted with FGS also has no ΔV measurement, but we can use our Δm_{583W} value from the FGS observations discussed in section 2. Henry et al. (1999) have noted that the F583W filter in HST's FGSs nearly matches the Johnson V passband and provided a relation to convert Δm_{583W} to ΔV. Although their relation was derived for stars presumed to have solar metallicity, we assume that even if the *magnitudes* will be different for subdwarfs vs. main sequence stars, the *colors* between two stars in a system will not be drastically different. So, we assume $\Delta m_{583W} \approx \Delta V$ for G 006-026 BC.

6. The Empirical Mass-Luminosity Relation and Discussion

We plot the 10 low-metallicity subdwarfs discussed here as solid points on and empirical mass-luminosity relation shown in Figure 7. The masses come directly from Tables 1, 3 and 4, where in addition to the subdwarfs, main sequence stars with masses from Delfosse et al. (2000), Torres et al. (2010), and Benedict et al. (2016) are plotted in Figure 7. These main-sequence stars generally fall along the 1 Gyr theoretical isochrone from Baraffe et al. (2015), shown with a solid line.

The ages of low metallicity stars are primarily measured using nearby GCs. Recently, Bono et al. (2010) and Correnti et al. (2016) acquired deep optical and near-IR photometry from the ground and HST to extend the detected GC populations down to early M dwarfs. Many of these clusters/cool dwarfs have ages estimated to be around ∼11 Gyrs. In addition, Monteiro et al. (2006) measured the first ages for two cool field K subdwarfs via their white dwarf companions' cooling curves, and found that these likely thick disk subdwarfs have ages of 6–9 Gyr.

However, until we can link the origins of these field subdwarfs to nearby GCs, we conservatively adopt 6 Gyr as the age for the all nearby subdwarfs. We sketch 6 Gyr isochrones for stars with [m/H] = −0.5, −1.0, and −2.0 from BT-Settl isochrones (Baraffe et al. 2015) in Figure 7 to permit comparisons to the empirical points for the subwarfs. According to the models, low metallicity subdwarfs appear brighter in M_V than dwarfs at a given mass, or alternately, are less massive for a given M_V.

Systems like μ Cas AB and GJ 704 AB are clearly seen above the mass-luminosity relation of main sequence stars. The locations of μ Cas A and B, which have [m/H] = −0.71, are well-matched to the model predictions for stars with [m/H] = −1.0 at an age of 6 Gyr. The metallicity of GJ 704 AB appears much lower ([m/H]< −1.0) than what has been measured [Fe/H]=−0.58, but the two subdwarfs certainly appear to be of lower

metallicity than main sequence stars. We note that Kennedy et al. (2012) used *Herschel's* Photodetector and Array Camera and Spectrometer (PACS) at 100 and 160 μm to reveal a rare and convincing circumbinary polar-ring debris disk around GJ 704 AB. This makes this system very unusual because this disk has somehow been maintained or created around a presumably old subdwarf binary. M_V values used in Figure 7 for GJ 704 A and B do not include any adjustment for obscuration by the disk, which is likely to be minimal. If such an adjustment is required, the points would move to brighter M_V, and the locations of the points would be towards even lower metallicity.

The remaining subdwarfs systems generally fall along the low metallicity curves. Because of the large mass errors of HIP 85209 AB and HIP 95575 AB measured by Horch et al. (2015), it is difficult to make a direct comparison between observations and models. Latham et al. (1992) reported a metallicity for HIP 85209 AB (HD 157948 AB) of [m/H]=−0.75, whereas Goldberg et al. (2002) reported [m/H]=−0.5. Horch et al. (2006) measured the dynamical masses of these subdwarfs using FGS, and determined via comparisons to the theoretical Yale-Yonsei models that the system should have metallicity close to −0.5. We note that the mass errors for HIP 85209 A and B are relatively large, so these two stars do not place strict constraints on the models.

Finally, both components in the new system described in this paper, G 006-026 B and C, merge with points for main sequence stars with solar metallicity in the MLR. This presents a conflict with the low metallicity measurements discussed in Section 1 — the points should lie near the [m/H] = −0.5 or −1.0 lines in Figure 7. For example, Carney et al. (1994) used high S/N echelle spectrograph to determine the metallicity of the primary in the system G6-26A, which is also a SB2 binary with a period of 8.7 days (Goldberg et al. 2002). They discussed the challenges of measuring the metallicities of SB2 binaries in detail, but there is no flag of the system regarding quality of their result of [m/H]

= −0.88. Casagrande et al. (2011) and Holmberg et al. (2009) used photometry of the unresolved primary to determine [Fe/H] = −0.52 and −0.60, respectively, thereby providing results that are match Carney's, again indicating that the system is metal-deficient.

In order to move the masses of B and C components to the low metallicity region, B component's mass would need to be reduced to ∼0.3 $M_\odot$ (62.7% of 0.478 $M_\odot$) to fall on the −0.5 metallicity curve on Figure 7. In Kepler's Third Law, such a mass decrease requires that the semi-major axis drop by 15%. There would then be a corresponding reduction in the projected separation (ρ) measured using FGS. Figure 8 shows an example of changing the projected separation along the X-axis by 15% while comparing to our best fitted S-curve. Note the poor fit to the FGS data, compared to the much better correct fit. In addition, because our orbital parallax matches that from Hipparcos, it is difficult to change the semi-major axis of this system from our derived value of 10.8 mas. Given that it is hard to dispute the three independent metallicty measurements or shrink the separation between B and C, we are left with no easy answer to the conundrum that that two points do not fall on the MLR where they should.

Given the overall trend that subdwarf systems are elevated in the mass-luminosity relation and match with the model, but there are several confounding factors that challenge observational programs focusing on mapping the mass-luminosity relation for subdwarfs, including (1) metallicity errors may be large because all available subdwarf binaries have separations less than 1″, so the acquired spectra used to determine metallicities are for two objects, not one, with consequent complications when measuring linewidths (G 006-026 AB is the only system to have an early type primary, which can be used to determine metallicity independently.), (2) mass errors are large because subdwarfs are rare and further away than comparable main sequence systems in the solar neighborhood, so parallax errors are larger, (3) accurate ΔV measurements are not available for a few systems and conversions from

other filters are imperfect (although overall, this is not likely to be a major problem), (4) not all of the systems are of the same age, so comparison to a single isochrone for 6 Gyr-old systems may not be appropriate.

This work shows that building an empirical mass-luminosity relation for subdwarfs has just begun. Only two subdwarf systems, μCas AB and GJ 704 AB, are clearly off the metallicity curves for main-sequence stars and have low mass errors, so there remains significant work to do in understanding the astrophysics that drives the locations of low metallicity stars on the mass-luminosity relation. We can make progress in our understanding of these Galactic fossils, as well as the star formation history and mass distribution of stars in the Milky Way, by discovering more subdwarf binaries for which high-quality metallicities, luminosities, and masses can be measured.

7. Acknowledgments

We thank D. Latham and A. Bieryla to provide us their unpublished metallicity of GJ 704 AB. We also thank the anonymous referee to provide us very valuable comments to improve this manuscript. The HST-FGS observations were supported for program number 10927 and 12561 by NASA through grants from the Space Telescope Science Institute, which is operated by the Association of Universities for Research in Astronomy, Inc., under NASA contract NAS5-26555.

This research has made use of the SIMBAD database, operated at CDS, Strasbourg, France. This work also has used data products from the Two Micron All Sky Survey, which is a joint project of the University of Massachusetts and the Infrared Processing and Analysis Center at California Institute of Technology funded by NASA and NSF. This research has made use of the Washington Double Star Catalog maintained at the U.S. Naval

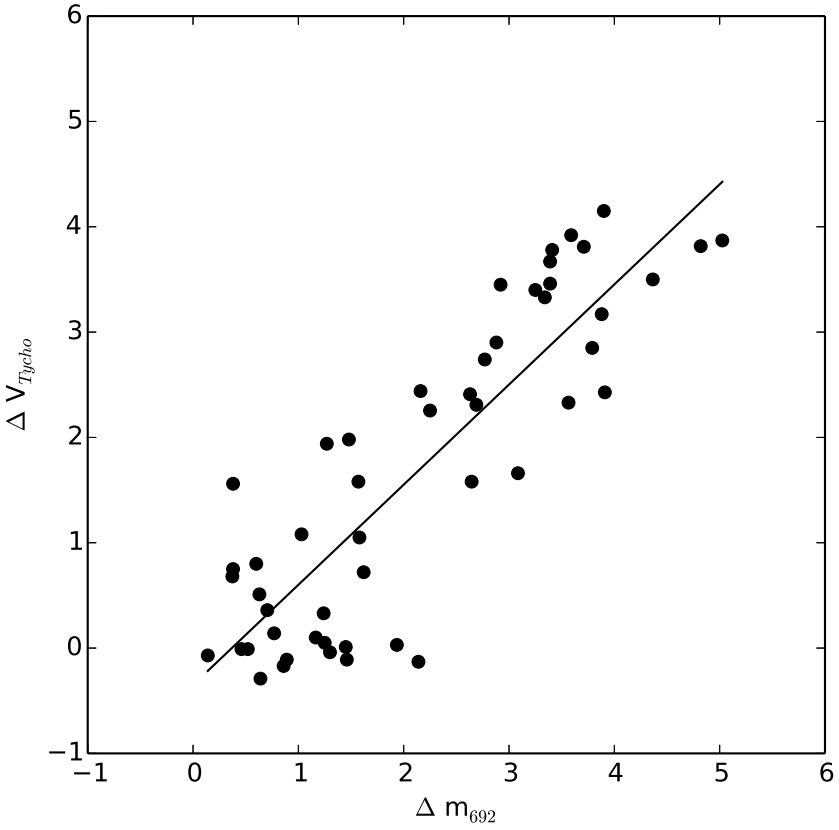

Fig. 6.— Relation ΔV_{Tycho} vs Δm_{692} from 51 binaries in Washington Double Star Catalog. The solid straight line is a fit ($\Delta V_{Tycho} = -0.35 + 0.95 \times \Delta m_{692}$) for these points.

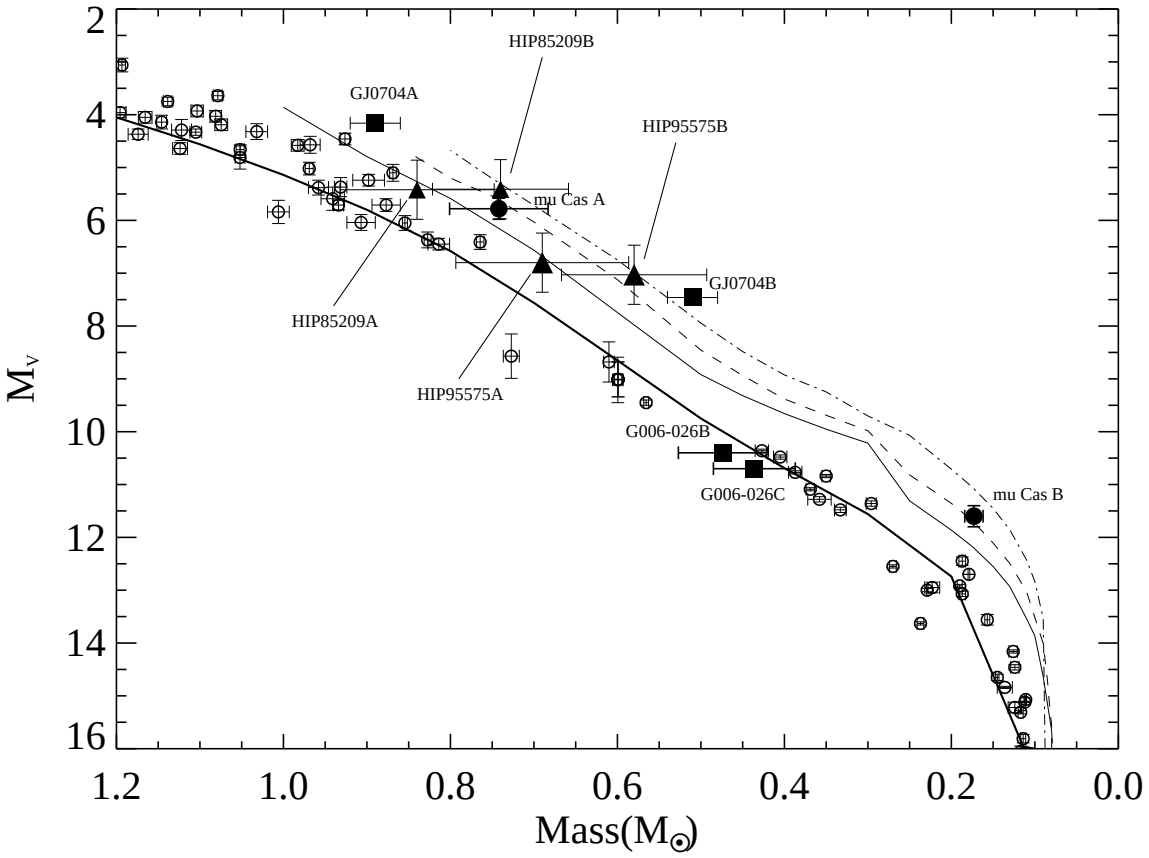

Fig. 7.— The mass-luminosity relation for subdwarfs (filled symbols) and dwarfs (open circles). Names are given for subdwarfs. Open circles are from Delfosse et al. (2000), Torres et al. (2010), and Benedict et al. (2016). Subdwarfs from Horch et al. (2015) are filled triangles, with a different sizes used simply to match the two stars in a system. Filled circles represent μ Cas AB and filled boxes represent the two systems discussed in detail in this paper, GJ 704 AB and G 006-026 BC. The thick solid line represents the main-sequence isochrone for age 1 Gyr from BT-settl (Baraffe et al. 2015). The three other lines represent the predicted locations of stars with metallicities of [m/H]=−0.5, −1.0 and −2.0 at an age of 6 Gyr from bottom to top, taken from Baraffe et al. (2015)

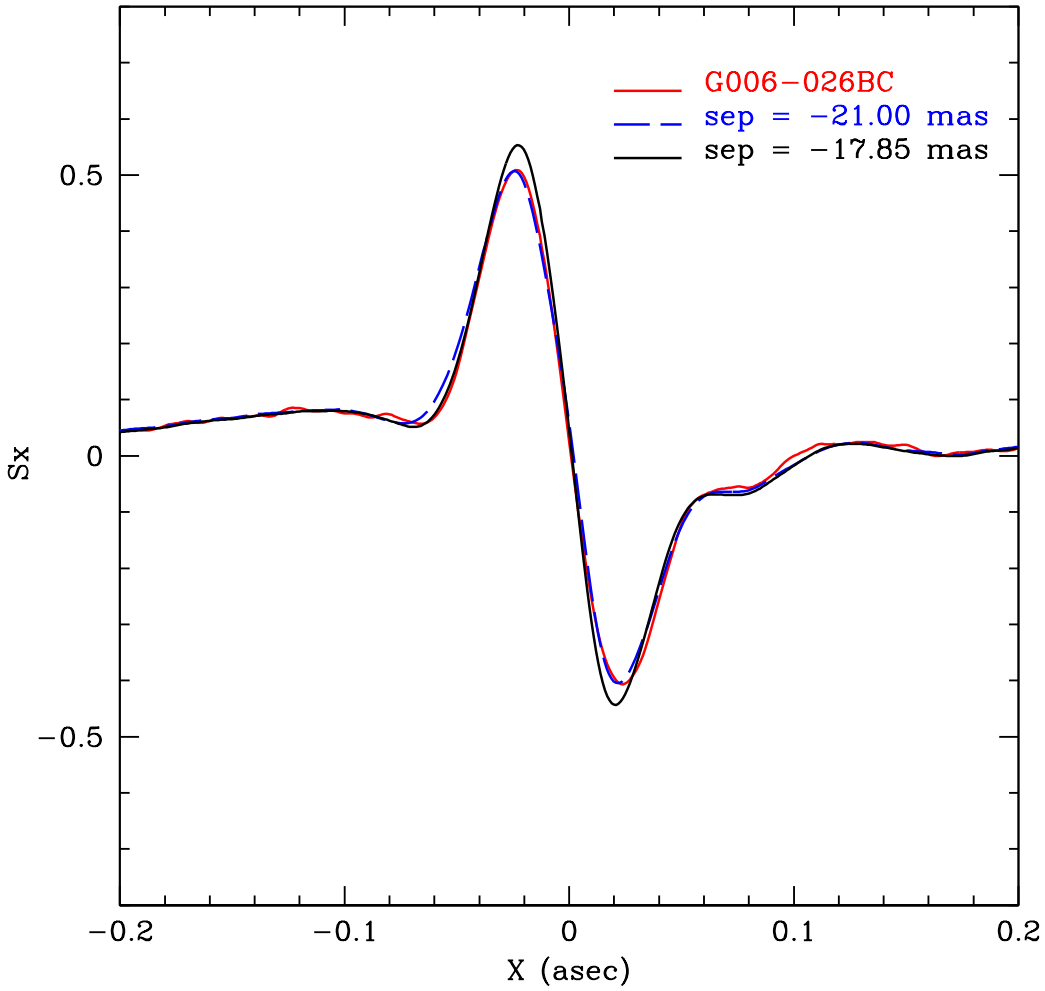

Fig. 8.— Displayed is the best fitting model (blue line) to the 2013.09 observation of G 006-26 BC (red line) along the FGS X-axis, with an angular separation of -21.0 mas. Also displayed is a model with an angular separation = -17.85 mas (black line), which would have resulted in the B component mass of ∼0.3 $M_{\odot}$ on the -0.5 theoretical metallicity line of the mass luminosity relation. Clearly this is inconsistent with the observation.

Observatory.

REFERENCES

Abt, H. A., & Willmarth, D. 2006, ApJS, 162, 207

Baraffe, I., Homeier, D., Allard, F., & Chabrier, G. 2015, A&A, 577, A42

Benedict, G.F., et al, 2016, private communication

Bono, G., Stetson, P. B., VandenBerg, D. A., et al. 2010, ApJ, 708, L74

Carney, B. W., Latham, D. W., Laird, J. B., & Aguilar, L. A. 1994, AJ, 107, 2240

Casagrande, L., Schönrich, R., Asplund, M., et al. 2011, A&A, 530, A138

Correnti, M., Gennaro, M., Kalirai, J. S., Brown, T. M., & Calamida, A. 2016, ApJ, 823, 18

Delfosse, X., Forveille, T., Ségransan, D., et al. 2000, A&A, 364, 217

Drummond, J. D., Christou, J. C., & Fugate, R. Q. 1995, ApJ, 450, 380

Duquennoy, A., Mayor, M., & Halbwachs, J.-L. 1991, A&AS, 88, 281

The *Hipparcos* and Tycho Catalogues, 1997, ESA SP-1200 (Noordwijk: ESA)

Gizis, J. E. 1997, AJ, 113, 806

Goldberg, D., Mazeh, T., Latham, D. W., et al. 2002, AJ, 124, 1132

Gudehus, D. H. 2001, Bulletin of the American Astronomical Society, 33, 850

Halbwachs, J.-L., Arenou, F., Famaey, B., et al. 2012, SF2A-2012: Proceedings of the Annual meeting of the French Society of Astronomy and Astrophysics, 87

Hartkopf, W. I., Mason, B. D., & Worley, C. E. 2001, AJ, 122, 3472

Heintz, W. D. 1972, AJ, 77, 160

Henry, T. J., Franz, O. G., Wasserman, L. H., et al. 1999, ApJ, 512, 864

Høg, E., Fabricius, C., Makarov, V. V., et al. 2000, A&A, 355, L27

Holmberg, J., Nordström, B., & Andersen, J. 2009, A&A, 501, 941

Horch, E. P., Franz, O. G., Wasserman, L. H., & Heasley, J. N. 2006, AJ, 132, 836

Horch, E. P., van Altena, W. F., Demarque, P., et al. 2015, AJ, 149, 151

Ibukiyama, A., & Arimoto, N. 2002, A&A, 394, 927

Jao, W.-C., Henry, T. J., Subasavage, J. P., et al. 2005, AJ, 129, 1954

Jao, W.-C., Henry, T. J., Beaulieu, T. D., & Subasavage, J. P. 2008, AJ, 136, 840

Jao, W.-C., Mason, B. D., Hartkopf, W. I., Henry, T. J., & Ramos, S. N. 2009, AJ, 137, 3800

Jao, W.-C., Henry, T. J., Subasavage, J. P., et al. 2011, AJ, 141, 117

Kaluzny, J., Thompson, I. B., Rozyczka, M., Pych, W., & Narloch, W. 2014, Acta Astron., 64, 309

Kaluzny, J., Thompson, I. B., Dotter, A., et al. 2015, AJ, 150, 155

Karaali, S., Bilir, S., Karataş, Y., & Ak, S. G. 2003, PASA, 20, 165

Kennedy, G. M., Wyatt, M. C., Sibthorpe, B., et al. 2012, MNRAS, 421, 2264

Korotin, S., Mishenina, T., Gorbaneva, T., & Soubiran, C. 2011, MNRAS, 415, 2093

van Leeuwen, F. 2007, A&A, 474, 653

Latham, D. W., Mazeh, T., Stefanik, R. P., et al. 1992, AJ, 104, 774

Latham, D. W. and Bieryla, A. 2016, private communication

Lodieu, N., Zapatero Osorio, M. R., & Martín, E. L. 2009, A&A, 499, 729

Lépine, S., Rich, R. M., & Shara, M. M. 2007, ApJ, 669, 1235

Maldonado, J., Eiroa, C., Villaver, E., Montesinos, B., & Mora, A. 2012, A&A, 541, A40

Malkov, O. Y., Tamazian, V. S., Docobo, J. A., & Chulkov, D. A. 2012, A&A, 546, A69

Mamajek, E. E., Meyer, M. R., & Liebert, J. 2002, AJ, 124, 1670

Mason, B. D., Wycoff, G. L., Hartkopf, W. I., Douglass, G. G., & Worley, C. E. 2015, VizieR Online Data Catalog, 1, 2026

McCarthy, D., Jr., Hancock, T., Freeman, J., et al. 1993, AJ, 105, 652

Monteiro, H., Jao, W.-C., Henry, T., Subasavage, J., & Beaulieu, T. 2006, ApJ, 638, 446

Ren, S., & Fu, Y. 2013, AJ, 145, 81

Ryan, S. G. and Norris, J. E., 1991, AJ, 101, 1835

Savcheva, A. S., West, A. A., & Bochanski, J. J. 2014, ApJ, 794, 145

Söderhjelm, S. 1999, A&A, 341, 121

Torres, G., Andersen, J., & Giménez, A. 2010, A&A Rev., 18, 67

Takeda, Y., & Takada-Hidai, M. 2013, PASJ, 65,

Watson, L. C., Pritchard, J. D., Hearnshaw, J. B., Kilmartin, P. M., & Gilmore, A. C. 2001, MNRAS, 325, 143

van Altena, W. F., Lee, J. T., & Hoffleit, D. 1995, The General Catalogue of Trigonometric Stellar Parallaxes (4th ed.; New Haven: Yale Univ. Obs.)

This manuscript was prepared with the AAS LaTeX macros v5.2.